Pure appl. geophys. (2006) 1193–1213
0033–4553/06/071193–21
DOI 10.1007/s00024-006-0073-7

Pure and Applied Geophysics

Calibration of the Tibetan Plateau Using Regional Seismic Waveforms

Lupei Zhu[1], Ying Tan[2], Donald V. Helmberger[2], and Chandan K. Saikia[3]

Abstract—We use the recordings from 51 earthquakes produced by a PASSCAL deployment in Tibet to develop a two-layer crustal model for the region. Starting with their ISC locations, we iteratively fit the *P*-arrival times to relocate the earthquakes and estimate mantle and crustal seismic parameters. An average crustal *P* velocity of 6.2–6.3 km/s is obtained for a crustal thickness of 65 km while the *P* velocity of the uppermost mantle is 8.1 km/s. The upper layer of the model is further fine-tuned by obtaining the best synthetic *SH* waveform match to an observed waveform for a well-located event. Green's functions from this model are then used to estimate the source parameters for those events using a grid search procedure. Average event relocation relative to the ISC locations, excluding two poorly located earthquakes, is 16 km. All but one earthquake are determined by the waveform inversion to be at depths between 5 and 15 km. This is 15 km shallower, on average, than depths reported by the ISC. The shallow seismicity cut-off depth and low crustal velocities suggest high temperatures in the lower crust. Thrust faulting source mechanisms dominate at the margins of the plateau. Within the plateau, at locations with surface elevations less than 5 km, source mechanisms are a mixture of strike-slip and thrust. Most events occurring in the high plateau where elevations are above 5 km show normal faulting. This indicates that a large portion of the plateau is under EW extension.

Key words: The Tibetan Plateau, locations of regional earthquakes, earthquake moment tensors, crustal velocity model, waveform modeling.

1 Introduction

The main objective of this paper is to demonstrate the usefulness of temporary seismic recording deployments in calibrating regional paths so that Green's functions can be used effectively in real-time seismic monitoring systems. The characterization of seismic activity is becoming increasingly important in many ways, from monitoring and developing tectonic kinematics to generating effective shake-maps (Kanamori *et al.,* 1999). While local propagation effects can be extremely complex, especially at short periods, signals in the period range of 2–10 s remain stable over local geological provinces. Thus, local 1-D model Green's functions can work quite well in many places. Adding path-specific timing corrections then allows a few

[1] Department of Earth and Atmospheric Sciences, Saint Louis University, St Louis, Missouri, USA. E-mail: lupei@eas.slu.edu
[2] Seismological Laboratory, California Institute of Technology, Pasadena, California, USA
[3] URS Co., Pasadena, California, USA

broadband stations, in combination with a few travel-time picks and first-motion polarities from other stations, to be used effectively in source characterization. This and a companion paper (TAN *et al.,* 2006) will demonstrate the effectiveness of this methodology.

We will use waveform data collected in a Sino-US PASSCAL seismic recording experiment on the Tibetan Plateau (OWENS *et al.,* 1993). In the one-year long experiment from July 1991 to July 1992, 11 broadband digital seismic stations were deployed (Fig. 1). Except for station TUNL where a Guralp sensor was installed, all stations were equipped with STS-2 sensors. The large amount of high quality data from this experiment provided, for the first time, a unique opportunity to study seismic activity of the Tibetan Plateau, one of the most interesting structures on Earth. We will concentrate on deriving the best average 1-D velocity model for the

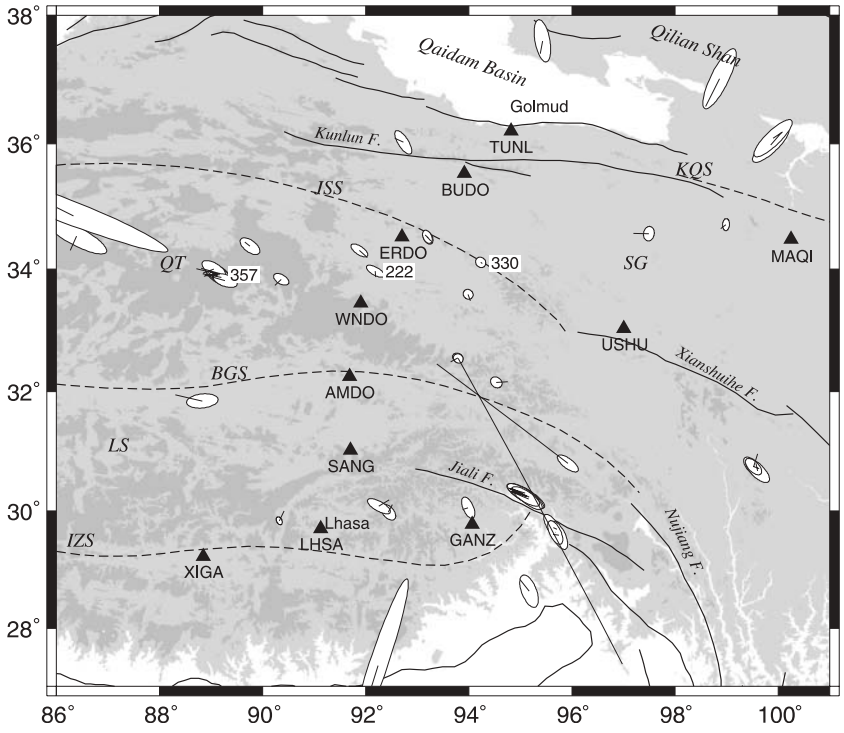

Figure 1

Topography (light and dark grays represent areas 3 and 5 km above sea-level, respectively), and major faults (solid curves) in central and eastern Tibet. The plateau is divided into several terranes separated by sutures (dashed lines); BGS: Bangong Suture; IZS: Indo-Zangbu Suture; JSS: Jinsha Suture; KQS: Kunlun-Qinling Suture; LS: Lhasa Terrane; SG: Songpan-Ganzi Terrane; QT: Qiangtang Terrane. Triangles represent eleven broadband stations of the 1991–92 Sino-US PASSCAL experiment. Ellipses represent 51 relocated earthquakes using their first arrivals. The ellipsis sizes are determined by 1-σ's of relocation uncertainties. Their offsets relative to their ISC locations are indicated by straight lines.

plateau. This is achieved by using travel times of various regional phases and matching waveforms. Source mechanisms and depths are then determined for 51 earthquakes using the Cut-and-Paste (CAP) method (ZHU and HELMBERGER, 1996b). We refer to these pure double-couple solutions as regional fault parameters (RFP), to distinguish them from other source estimates, such as long-period CMT solutions.

2. Tectonic Setting and Previous Results

The Tibetan Plateau is the youngest plateau in the world. It is estimated that the present elevation of much of the plateau was attained only 8 to 11 million years ago (HARRISON *et al.,* 1992; MOLNAR *et al.,* 1993). The plateau is surrounded by several Precambrian cratons with large-scale thrust and strike-slip faults serving as boundaries. Despite its uniform elevation, the plateau consists principally of three terranes that were accreted successively to Eurasia during the Mesozoic Era (DEWEY *et al.,* 1988). They are, from north to south, the Songpan-Ganzi Terrane, the Qiangtang Terrane, and the Lhasa Terrane as denoted in Figure 1. This division is mostly based on the recognition of several ophiolite zones that are interpreted as sutures (DEWEY *et al.,* 1988; YIN and NIE, 1996).

Before the 1991–1992 PASSCAL experiment, many seismic studies measured group and/or phase velocities of surface waves propagating across the plateau and invert for 1-D velocity structure (ROMANOWICZ, 1982; JOBERT *et al.,* 1985; BRANDON and ROMANOWICZ, 1986). Others used *Pn* and *Sn* travel times to estimate velocities in the uppermost mantle (CHEN and MOLNAR, 1981; BARAZANGI and NI, 1982). There were also several deep seismic sounding profiles in southern and central Tibet by Chinese and French scientists (TENG *et al.,* 1983; HIRN *et al.,* 1984a,b; LU and WANG, 1990). Upper mantle structure down to 400 km beneath the plateau was investigated using *S* waves in the distance range of 15° to 30° (LYON-CAEN, 1986; ZHAO *et al.,* 1991). The results from some of these studies have been summarized by MOLNAR 1988. In general, all of them show a thick crust (50 to 80 km) with high uppermost mantle velocities of 8.1 to 8.4 km/s for *Pn* and 4.6 to 4.8 km/s for *Sn*. The average velocities of lithospheric mantle in this region are low, particularly under north-central Tibet. Many studies also emphasize lateral variation. For example, surface wave studies indicate a thinner crust in north-central Tibet. Strong attenuation of high-frequency *Sn* exists in the same region (NI and BARAZANGI, 1983).

The 1991–1992 Sino-US experiment provided a data set to study the plateau structure using both earthquakes and receivers within the plateau. MCNAMARA *et al.* (1995) used 371 *Pn* arrival times of 61 Tibetan earthquakes recorded by the array and obtained a *Pn* velocity of 8.16 ± 0.07 km/s. There is also a 4% velocity variation between the northern and the southern part. RODGERS and SCHWARTZ (1997)

estimated average crustal and uppermost mantle velocities of the plateau by modeling *Pnl* waveforms from a few large regional earthquakes. They found a *Pn* velocity of 8.2 km/s beneath a 70 km thick crust in southern Tibet. The crust of northern and central Tibet (the Qiangtang Terrane) has a lower average velocity (6.2 km/s), lower *Pn* velocity (8.1 km/s) and a crustal thickness of 65 ± 5 km (RODGERS and SCHWARTZ, 1998).

Since 1992, there have been several more seismic experiments conducted on the Tibetan plateau, including the International Deep Profiling of Tibet and the Himalaya (INDEPTH, phases I–III) (e.g., ZHAO *et al.,* 1993,2001; NELSON *et al.,* 1996) and the 1993 and 1998 Sino-French passive seismic experiments (e.g., WITTLINGER *et al.,* 1996; VERGNE *et al.*, 2002). The INDEPTH-III wide-angle and vertical seismic reflection data show that the crust of central Tibet is about 65-km thick without significant Moho offset in the vicinity of the Bangong Suture. The average crustal *P*-wave velocity decreases from 6.3 km/s in southern Tibet to 6.2 km/s in northern Tibet (ZHAO *et al.,* 2001). The results are consistent with the crustal structure obtained from surface wave dispersion analysis (RAPINE *et al.,* 2003). In addition, the wide-angle seismic data and the surface wave study indicate a high-velocity lower crust in southern Tibet. LANGIN *et al.* (2003) relocated 267 local earthquakes within 400 km of the INDEPTH-III array. They found that events tend to be more clustered in or near large grabens and strike-slip faults after relocation. 99% of the earthquakes are shallower than 25 km. The majority of the 50 focal mechanisms obtained from first-motion polarities are normal and strike-slip faulting and are consistent with results of previous studies (e.g., MOLNAR and LYON-CAEN, 1989; RANDALL *et al.,* 1995).

3. Event Relocation Using P Arrivals

During the one-year experiment the array recorded about 100 earthquakes listed in the International Seismological Centre (ISC) Bulletin with distances less than 1000 km. For the purpose of deriving a 1-D velocity model for the plateau, we excluded events that are outside the plateau to avoid possible path contamination. We selected 51 earthquakes, all of which were recorded by at least four stations with clear *P* onsets. We measured *P* onsets for all 51 events, obtaining 391 picks. Their travel times vs. epicentral distances using their ISC origin times and locations (listed in Table 1) are plotted in Figure 2. The large scatter is mostly attributed to the unreliable locations and origin times in the catalog. The m_b magnitudes of these events are between 3.3 and 5.5, therefore the number of station reports used by the ISC is very limited. The abnormal crust of Tibet also causes bias in the ISC event origin times. Therefore, relocating these events is necessary before further travel-time analysis can be applied.

Table 1

Relocations and Focal Mechanisms (FM) of 51 Earthquakes

Event	ISC Origin Time and Location					Relocation				FM	
	Date	o, GMT	Lat./Long.	h,km	m_b	Lat./Long.	Δo,s	Δx^a	h,km	M_w	$\phi/\delta/\lambda$
199	91/07/18	13:24:56.9	30.37/95.00	9	4.9	30.42/94.71	1.4	12	5	4.1	160/21/−71
201	91/07/20	19:02:28.3	30.39/95.00	5	4.7	30.42/94.81	0.6	3	5	4.0	170/23/−63
204	91/07/23	16:51:51.8	30.33/95.00	13	4.7	30.41/94.78	0.2	10	5	4.1	157/21/−70
205	91/07/24	06:06:43.8	30.38/95.00	21	4.7	30.44/94.69	−1.2	11	5	3.9	151/19/−82
206	91/07/25	01:52:43.7	30.39/95.00	16	4.7	30.38/94.64	0.0	11	5	3.8	158/22/−70
209	91/07/28	23:58:20.5	30.34/95.00	33	4.8	30.40/94.74	−3.1	9	5	4.0	160/22/−70
210	91/07/29	15:48:07.5	30.34/95.00	20	4.6	30.42/94.69	−0.4	15	5	4.0	161/23/−71
211	91/07/30	22:22:05.3	30.37/95.00	25	4.6	30.43/94.74	−1.9	9	5	3.9	161/21/−71
222	91/08/10	20:21:52.7	33.87/92.00	15	4.5	33.97/92.18	−0.2	11	10	4.7	252/83/2
239	91/08/27	05:14:34.4	34.18/92.00	33	3.3	34.37/91.84	−3.7	27	9	4.1	256/66/−8
242	91/08/30	14:32:12.1	34.57/97.00	18	4.3	34.60/97.56	−0.6	34	5	4.0	96/69/−15
245	91/09/02	11:05:50.5	37.41/95.00	10	5.3	37.77/95.57	−3.5	44	12	4.7	102/61/79
251	91/09/08	23:54:42.3	36.59/99.00	27	4.6	36.71/98.66	−2.4	15	5	4.2	269/58/80
252	91/09/09	21:54:51.7	28.84/95.00	0	4.7	28.69/94.94	−3.4	17	21	4.3	241/29/12
255	91/09/12	23:06:30.7	29.69/96.00	38	4.5	29.68/95.62	−3.4	9	5	4.0	10/53/89
263	91/09/20	11:16:11.7	36.18/100.00	13	5.4	36.24/100.16	−0.9	12	12	4.9	99/76/60
270a	91/09/27	07:39:54.3	34.65/99.00	21	4.5	34.77/99.02	−0.8	18	5	4.1	329/33/82
270b	91/09/27	11:56:40.7	30.00/90.00	33	3.7	29.82/90.36	−2.1	21	5	3.6	64/56/−11
270c	91/09/27	23:31:21.5	32.45/93.00	33	4.3	30.91/95.63	−16.2	274	14	3.8	107/72/33
283	91/10/10	00:39:06.1	34.44/90.00	33	4.2	34.50/89.60	−3.7	9	5	4.3	29/62/−59
323	91/11/19	01:04:18.0	32.48/94.00	33	4.3	32.49/93.82	−1.5	16	8	4.0	21/38/−89
325	91/11/21	13:37:43.8	33.74/90.00	48	4.0	34.02/90.14	−5.2	32	5	4.5	251/60/−16
328	91/11/24	07:35:26.2	34.01/89.00	29	4.1	34.04/88.94	−4.2	21	5	4.1	221/31/−67
329	91/11/25	10:08:39.4	34.01/89.00	32	4.2	34.02/88.89	−4.3	8	5	4.3	222/33/−64
330a	91/11/26	15:31:14.8	33.88/89.00	33	4.3	33.99/88.92	−4.6	12	5	4.2	211/32/−72
330b	91/11/26	21:16:00.0	34.09/94.00	31	4.2	34.14/94.27	−1.8	6	11	4.4	286/63/−21
336	91/12/02	19:45:38.1	32.16/95.00	57	4.2	32.10/94.56	−3.2	20	10	4.1	43/73/−74

Table 1

(Contd.)

Event	ISC Origin Time and Location					Relocation				FM	
	Date	o, GMT	Lat./Long.	h,km	m_b	Lat./Long.	Δo,s	Δx^a	h,km	M_w	$\phi/\delta/\lambda$
348	91/12/14	08:20:23.7	33.92/89.00	31	5.1	34.04/88.83	−4.7	13	5	4.8	212/30/−72
349	91/12/15	15:59:34.3	30.03/94.00	33	4.3	30.14/93.88	−2.5	13	8	4.0	211/69/−9
351	91/12/17	20:27:47.8	33.96/89.00	15	4.3	34.04/88.83	−3.0	17	5	4.2	222/24/−61
357a	91/12/23	01:58:25.0	33.90/89.00	31	5.2	34.05/88.84	−4.5	17	5	4.8	210/31/−70
357b	91/12/23	02:14:56.0	33.90/89.00	47	4.8	34.01/88.86	−5.3	16	5	4.5	−2/60/−87
358	91/12/24	21:27:50.9	30.11/93.00	19	4.4	29.98/92.41	0.9	18	10	4.1	22/54/−79
360	91/12/26	13:24:18.8	30.96/100.00	33	4.1	30.92/99.50	0.6	10	10	4.1	300/78/8
365	91/12/31	21:14:15.8	30.81/100.00	5	4.3	30.91/99.67	1.9	15	12	4.2	294/67/−2
002	92/01/02	02:35:38.4	33.94/89.00	48	4.6	34.09/88.76	−7.0	19	5	4.4	221/30/−56
008	92/01/08	17:41:39.9	30.19/92.00	14	3.9	30.00/92.32	1.8	25	10	3.9	40/54/−69
023	92/01/23	10:26:25.8	34.55/93.00	19	4.0	34.52/93.21	−1.4	6	5	4.2	280/67/43
034	92/02/03	15:44:22.6	34.45/93.00	10	4.9	34.60/93.23	0.1	17	5	4.5	107/19/53
037	92/02/06	03:35:15.0	29.61/96.00	15	5.5	29.71/95.66	0.0	12	5	5.0	0/61/60
040	92/02/09	12:44:52.8	29.64/96.00	9	4.9	29.74/95.68	0.5	11	5	4.4	352/35/47
076	92/03/16	01:18:56.4	34.30/86.00	36	4.4	34.50/86.33	−3.1	22	9	4.2	63/68/−29
090	92/03/30	18:29:47.7	27.39/97.00	33	3.9	32.53/93.82	21.0	645	8	3.7	31/39/−74
104	92/04/13	03:47:50.7	31.95/88.00	35	4.4	31.75/88.22	−5.4	23	5	4.5	227/49/−23
109	92/04/18	18:19:28.9	36.09/93.00	8	4.0	36.07/92.76	0.8	18	5	4.3	92/60/7
111	92/04/20	18:50:27.3	26.99/92.00	33	4.5	27.30/92.21	0.7	36	12	4.0	191/90/34
137	92/05/16	20:19:53.1	36.19/100.00	17	4.8	36.31/100.27	−2.1	21	14	4.4	110/64/80
139	92/05/18	19:55:39.0	34.85/86.00	33	4.0	34.79/86.53	−3.3	19	15	4.0	50/74/23
143	92/05/22	05:47:31.4	30.72/100.00	29	4.5	30.89/99.70	−0.5	20	5	4.0	299/44/−52
155	92/06/03	02:42:36.9	33.90/89.00	10	4.5	33.96/88.94	−0.2	7	8	4.2	30/48/−79

[a]Relocation offset in km with respect to the ISC location.

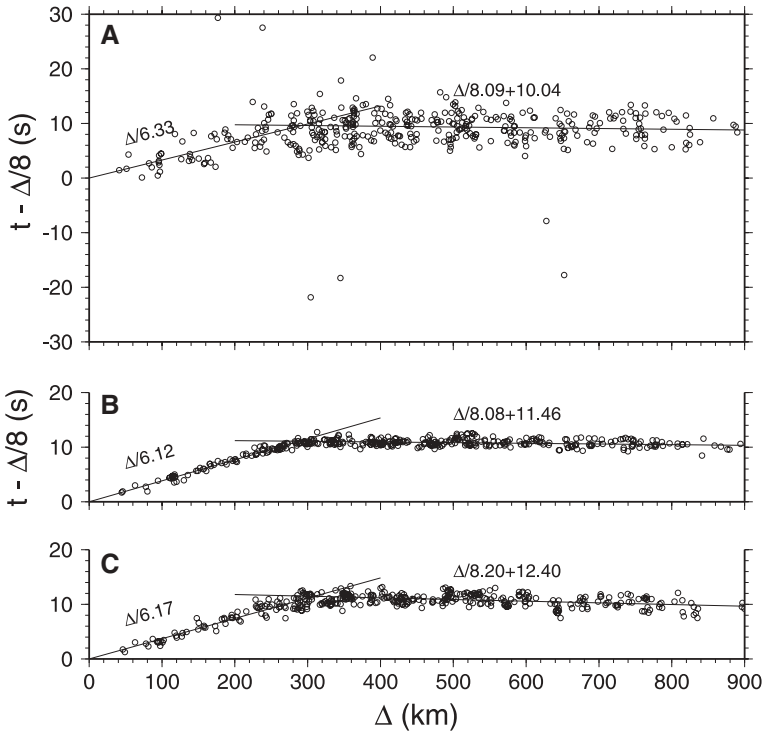

Figure 2
First *P* arrival travel times as a function of epicentral distance (A) using the ISC source locations and origin times; (B) using relocations by *P* arrivals; (C) using relocations by *P* arrivals and *S*-wave shifts, see text. Estimated *Pn* and *Pg* velocities are presented next to their branches.

Locating earthquake from arrival times is a classical nonlinear inversion problem in seismology. Most location methods simplify the problem by linearization using an *a priori* velocity model, usually one-dimensional. To account for heterogeneity in the shallow crust, some methods such as the Joint Hypocenter Determination (JHD) or the Progressive Multiple Event Location (PMEL) introduce station corrections and solve for event locations and station corrections simultaneously using multiple events (DOUGLAS, 1967; PAVLIS and BOOKER, 1983). The station corrections may even be made source region dependent (RICHARDS-DINGER and SHEARER, 2000). KISSLING *et al.* (1994) gave a ''recipe'' to obtain the ''best'' 1-D model through multiple steps of event relocations and velocity inversions starting from the *a priori* model(s). Nevertheless, all these methods demand sufficient information for establishing a good velocity model of study area and the linearization approximation makes the final results sensitive to preliminary locations of events. Although there are several crustal velocity models, such as M45 (ROMANOWICZ, 1982) or TIP (ZHAO *et al.*, 1991), that could be used for earthquake relocation in Tibet, we prefer relocating our

events without using any *a priori* velocity model because the travel-time data will be used later to derive a velocity model and we want to avoid bias that might be caused by the initial model.

We developed a simple but effective relocation method which does not require an *a priori* velocity model. Assuming a one-layer crustal velocity model, the first arrival time at station i from event j satisfies

$$t_{ij} = \begin{cases} p_n \Delta_{ij}(x_j, y_j) + t_n^0 + o_j & \text{if } \Delta_{ij} > \Delta_c, \\ p_g \Delta_{ij}(x_j, y_j) + t_g^0 + o_j & \text{if } \Delta_{ij} < \Delta_c, \end{cases} \quad (1)$$

where x_j, y_j, and o_j are the longitude, latitude, and origin time of the event; p_n and p_g are the apparent slownesses for *Pn* and *Pg* and t_n^0 and t_g^0 are the intercept times; Δ_{ij} is the epicentral distance and Δ_c is the cross-over distance. The relocation is formulated as an optimization problem to find the best (x_j, y_j, o_j) that minimizes the difference between observed and predicted travel times. Note that both event parameters (x_j, y_j, o_j) and velocity model parameters (p_n, t_n^0, p_g, t_g^0) are unknown. The problem is solved in two steps. First, using the ISC locations and origin times as the initial values of (x_j, y_j, o_j), model parameters (p_n, t_n^0, p_g, t_g^0) can be obtained by solving the above linear equations. Then we fix the velocity model parameters and look for the "best" event locations. This is done using a grid search surrounding the ISC locations, starting from the event with the largest *rms* of travel-time residuals. The procedure is repeated until a convergence is reached. Note that the second step is a nonlinear problem. The use of grid search avoids the linearization approximation thus greatly reducing the dependence of solution on initial event locations. This technique does not require an *a priori* velocity model but assumes that all events are located at the same depth. Since parameter o_j trades off with source depth, depth difference between events are absorbed into the origin time. Also, there is evidence that most earthquakes in Tibet occur at depths between 5 and 20 km (MOLNAR and CHEN, 1983; ZHAO and HELMBERGER, 1991; LANGIN *et al.,* 2003).

We applied the relocation method to the 391 *P* picks of the 51 events. We found that the algorithm is very efficient and is able to reach convergence after five iterations. We also tested the sensitivity of the final solution to the initial event locations by both randomly and systematically perturbing their ISC locations up to 30 km. The final locations and velocity model parameters remain the same. Figure 1 shows the relocation results. For events located within the array, relocation uncertainties are 5 to 10 km, based on the sizes of 1-σ uncertainty ellipses. Events outside the array have larger relocation uncertainties (10 to 50 km) and the ellipses are elongated in the direction toward the center of the array. This is due to a trade-off between epicentral distance and event origin time in our relocation algorithm. For most events, relocation offsets from their ISC locations are within relocation uncertainty, suggesting that they were reasonably well located by the ISC. However, there are a few well-relocated earthquakes which are more than 50 km away from their ISC locations (Fig. 1). Two events are relocated by more than 270 km. In the

ISC report, both events were recorded by fewer than 10 stations and are listed as "less reliable/poor solution" with travel-time residuals exceeding 10 s at some stations (INTERNATIONAL SEISMOLOGIVAL CENTR, 2001). The success of our method to locate these events which were mislocated by more than 100 km is not surprising, and is attributed to the elimination of linearization approximation. It also confirms the insensitivity of solution to events' initial locations.

4. 1-D Velocity Structure of Tibet and Lateral Variation

Model parameters p_n, t_n^0, and p_g estimated from the relocation are given in Figure 2. Our determination of *Pn* velocity (8.08 km/s) is consistent with previous results (CHEN and MOLNAR, 1981; MCNAMARA *et al.,* 1995; RODGERS and SCHWARTZ, 1998). The *Pg* velocity of 6.12 km/s is quite low and probably represents the *P*-wave velocity of the upper crust. From teleseismic receiver function studies (OWENS and ZANDT, 1997; YUAN *et al.,* 1997; ZHU, 1998) and regional seismic data analyses (RODGERS and SCHWARTZ, 1998; ZHAO *et al.,*2001, ROSS *et al.,* 2004), the average crustal thickness of the Tibetan plateau is about 65 km. Assuming a shallow source depth of 10 km and a crustal thickness of 65 km, we estimated the average crustal *P* velocity to be 6.3 km/s from the *Pn* intercept time, which agrees well with values from modeling *Pnl* waveforms (RODGERS and SCHWARTZ, 1998) and the INDEPTH-III wide-angle seismic survey (ZHAO *et al.,* 2001).

Because the shallow crustal structure has a strong influence on the propagation of regional Love and Rayleigh waves (e.g., SONG *et al.,* 1996), we divided the crust into two layers and use Love waveforms to invert for the thickness and *S* velocity of the top layer. We used a well recorded event (222, see Fig. 1). The source depth and mechanism of the event were taken from RANDALL *et al.* (1995). Synthetic seismograms were computed for a range of velocity models with different thicknesses and velocities. The *rms* of misfits between the observed waveforms and synthetics is shown in Figure 3. The elongated minimum area shows the trade-off between thickness and velocity, which is quite common for surface wave studies. The best model has a layer thickness of 4 km with an *S* velocity of 2.7 km/s. The model is consistent with the INDEPTH-III wide-angle seismic reflection result that shows a 4-km-thick sedimentary layer of *P* velocity of 4–5 km/s (ZHAO *et al.,* 2001).

The above 1-D model is used to determine source depths and focal mechanisms of all 51 events (see next section). After the source parameters are obtained, the events are relocated again by minimizing a weighted sum of L2-norms of *P*-wave travel-time residuals and *S*-wave time shifts between observations and synthetics. The *S*-wave time shifts are obtained by cross-correlating data and synthetics after aligning the two by the first-arrival. In other words, they are double differences of *S-P* travel times. They constrain epicentral distances, which is very helpful in reducing the trade-off between event origin time and distance, especially for events outside the

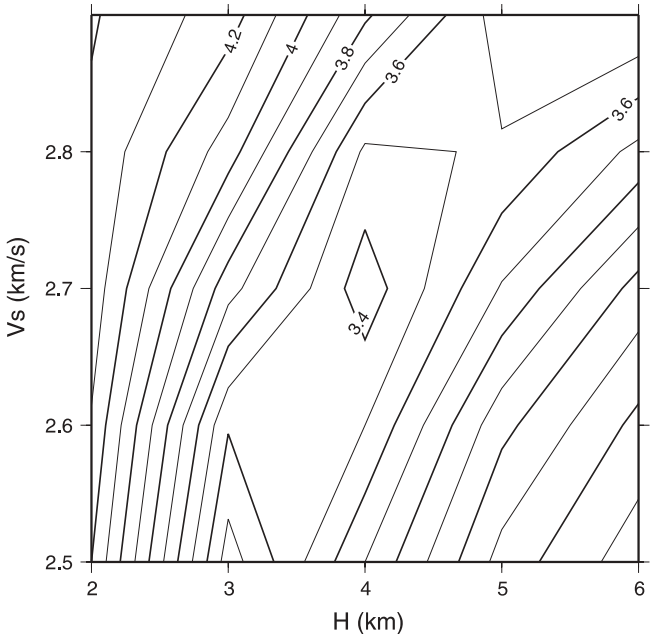

Figure 3
Waveform misfit errors between the *SH* waveforms of event 222 and synthetics using different thicknesses and *S*-wave velocities of the uppermost layer.

array. Two examples, one for event 330b, which is inside the array, and another for event 357 outside the array, are shown in Figure 4. We can see that by using *S*-wave time shifts relocation uncertainty of the outside event is greatly reduced. The final relocation results are shown in Figure 5 and are listed in Table 1.

The apparent velocities of *Pg* and *Pn* are re-estimated using the relocated events (Fig. 2C). Their values are slightly larger than previous estimates. The final velocity model T93 based on the above travel-time data and surface-wave modeling, and corrected for Earth's spherical geometry, is listed in Table 2. A crustal *Vp*/*Vs* ratio of 1.8 is used, based on teleseismic receiver function studies (ZHU, 1998).

After relocations that minimize *P* travel-time residuals and *S*-wave time shifts, there are still time shifts extending to $\pm$ 6 s between observed surface waves and synthetics (Fig. 6). They are interpreted as being caused by lateral velocity variations in the crust. We divided the region into 10-km-size cells and determine velocity perturbation of each cell by a tomographic inversion of the time shifts. A singular value decomposition (SVD) method is used to solve the travel-time perturbation equations with an added constraint of smoothness of velocity perturbations. The resulting velocity perturbations are displayed in Figure 6. Because the time shifts are derived by cross-correlating Rayleigh/Love surface waves with synthetics in the frequency range of 10 to 30 s, the velocity perturbation map shows effectively group

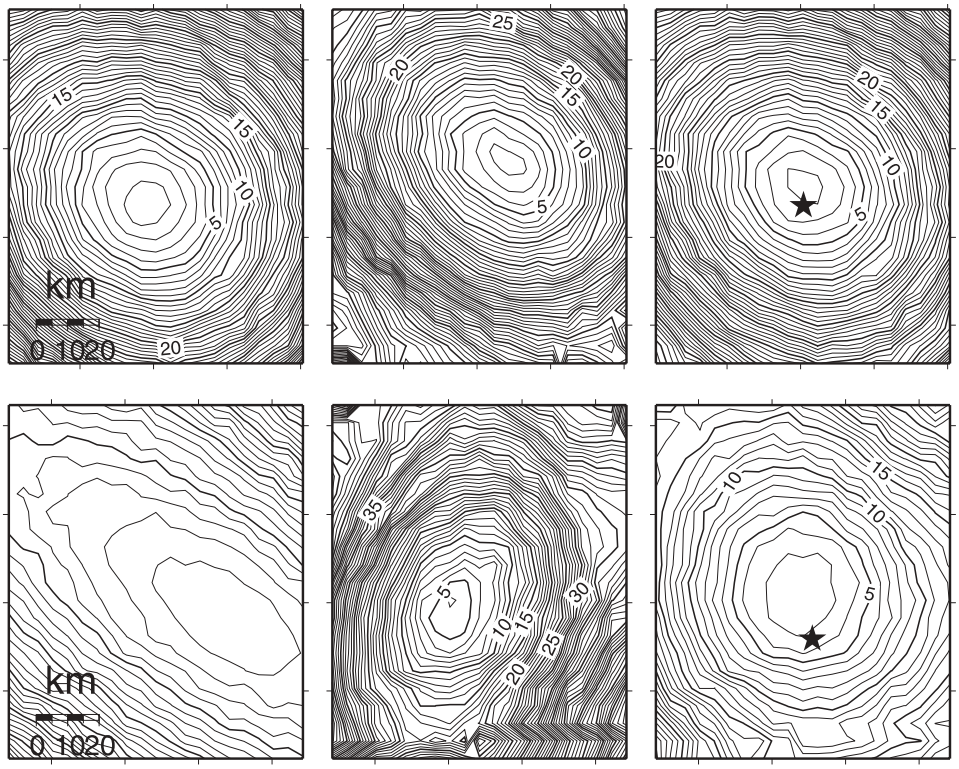

Figure 4
Contour plots of *rms* of *P* travel-time residuals (left), *S*-wave time shifts (middle), and a weighted sum of the two (right) for event 330b on the top and 357a on the bottom. Star represents the ISC location.

velocity perturbations of surface waves in this period range. The map shows low-velocity anomalies in the Qiangtang Terrane, which is consistent with previous studies (NI and BARAZANGI, 1983; MCNAMARA *et al.,* 1995; RODGERS and SCHWARTZ, 1998). We view this kind of map as a useful product of regional calibration to be used in conjunction with the 1-D regional model. It allows us to predict time shifts for locating and determining source parameters of future earthquakes. This will be demonstrated in TAN *et al.,* (2006).

5. Source Depths and Mechanisms of Tibetan Earthquakes

Green's functions for the 1-D model were computed for distance ranges and depths on a grid with 5-km spacing using a frequency-wavenumber (F-K) integration method (ZHU and RIVERA, 2000). We used a direct grid search technique to determine the source mechanisms and depths in which misfits in the *Pnl* (extended *P*

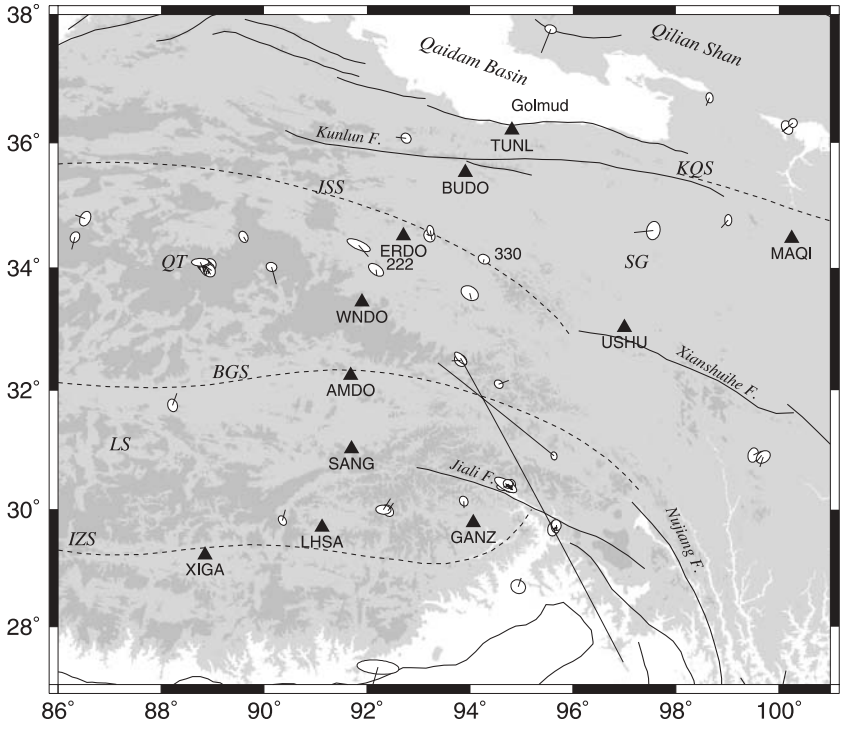

Figure 5
Relocation results using both first *P*-arrival travel times and *S*-wave time shifts.

wave) and surface waves are minimized separately. The approach was originally proposed by ZHAO and HELMBERGER (1994) and modified to handle data recorded by stations near nodes of radiation pattern by ZHU and HELMBERGER (1996b). One of the advantages of this approach is that it desensitizes the timing between principal crustal arrivals by fitting portions of the waveforms independently, allowing some time shifts between the observations and synthetics. Good source mechanism estimations can be obtained even when only imperfect Green's functions and earthquake locations are available.

Table 2

Velocity Model T93 of Tibet

Layer	Thickness, km	*Vp*, km/s	*Vs*, km/s
1	4	4.86	2.70
2	60	6.30	3.50
3	–	8.10	4.54

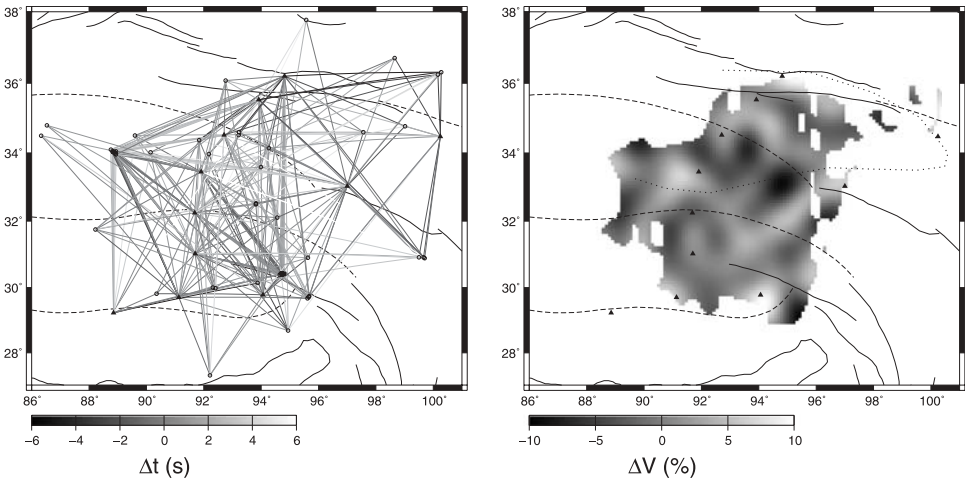

Figure 6
Surface wave time shifts from CAP inversion (left, positive shift means that the observation is later than predicted by the model) and the resultant surface wave velocity perturbations (right).

Figure 7 illustrates our RFP approach in which we present results pertaining to one event (330b) that occurred in the middle of our study area (Fig. 1). As shown in the figure, we have separated the *Pnl* portion from the surface waves. We low-pass filtered the surface waves up to 10 s and the *Pnl* waves to 3 s. We also multiplied the *Pnl* amplitudes by a factor of 2 to put more weighting on the body waves relative to the surface waves. The waveform fits of *Pnl* data and synthetics are shown on the left two columns. The next three columns show the waveform fits for surface waves. The numbers below each fit are the time shifts in seconds and the correlation coefficients (*cc*). Note that the *cc*'s for the *Pnl* observations beyond ~400 km are low because the *Pnl* waves are partially lost in noise. This means that the *SV*/*SH* ratio of the surface waves controls the solutions; a situation that works fine if there are at least two stations.

The focal mechanisms and depths of all events are listed in Table 1 and shown in Figure 8. Most all events are shallow (5 to 15 km). This is consistent with the result of LANGIN *et al.* (2003). Of the 51 events, RANDALL *et al.* (1995) determined moment tensors and depths of 37 events using long-period (>20 s) waveforms. In general, the two results agree well except for events 201, 210, 211, 023 and 104 (Table 1). Three of these events' moment tensor solutions were graded quality "C" in RANDALL *et al.* (1995), meaning that they have at least one of the P, T, or B axes relatively unconstrained. By including higher frequency signals in the inversion, we are able to place better constraints on focal mechanisms. The average difference between m_b and M_w is 0.25 magnitude unit with a mechanism dependence (Fig. 9). The strike-slip events exhibit m_b values that are lower than 0.5 magnitude unit than dip-slip events.

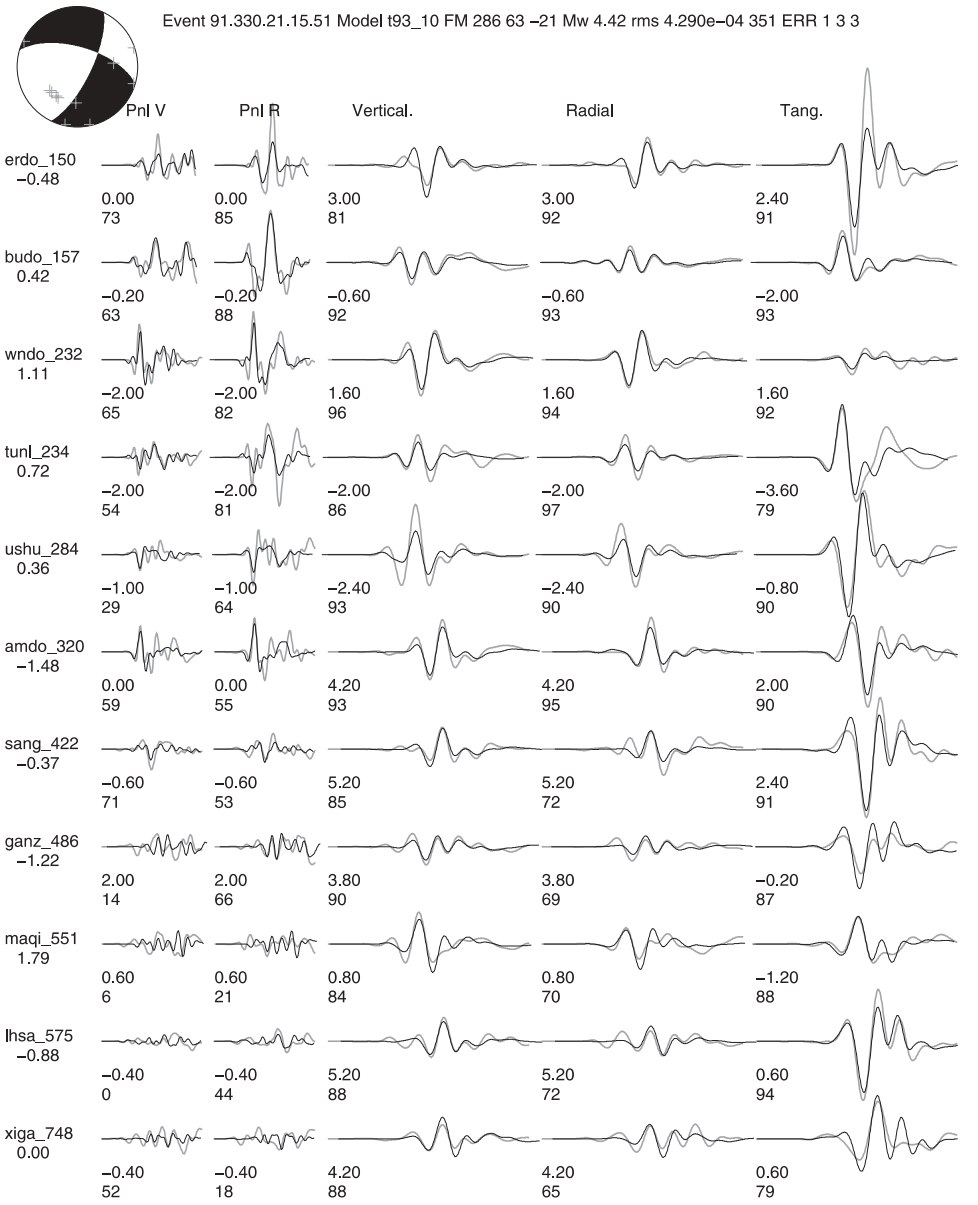

Figure 7

Displacement waveform fits for Event 330b. Data are shown in black with synthetics in gray color. Station names plus epicentral distances in km are given on the left. Their amplitudes are distance-decay compensated (r for the *Pnl*'s and $\sqrt{r}$ for the surface waves) and the *Pnl*'s are amplified by a factor of 2 relative to the surface waves. The time shift in seconds and cross-correlation coefficient are given below each waveform segment.

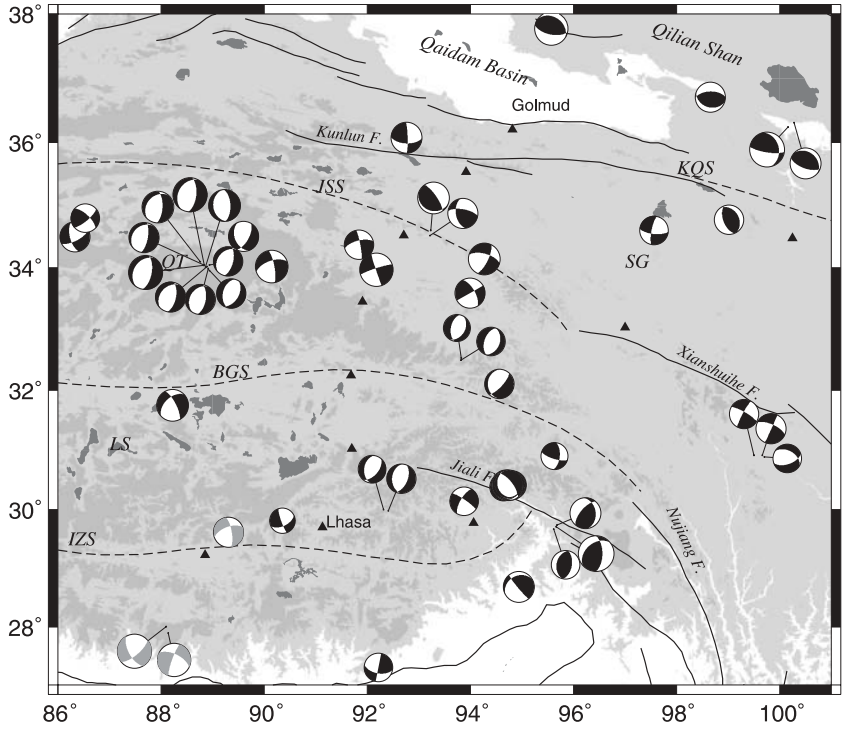

Figure 8
The lower-hemisphere projections of focal mechanisms of 51 earthquakes determined in this study and three subcrustal earthquakes (in gray shade) previously determined by ZHU and HELMBERGER (1996a).

This difference can be explained as being due to radiation pattern effects (HELMBERGER, 1983). A cluster of earthquakes northeast of station GANZ exhibit very large m_b:M_w differences of close to one magnitude unit; an intriguing anomaly noted by RANDALL *et al.* (1995). They also pointed out the complex earthquake faulting patterns of co-existing strike-slip, thrust, and normal faulting within a relative small geographic region. If we exclude this cluster there is in general a good correlation of focal mechanism with the epicenter elevation (Figs. 8 and 9). Along the margins of the plateau and in Qilian Shan where surface elevations are less than 4 km, thrusting events are dominant, reflecting ongoing crustal shortening in these regions. Source mechanisms are a mixture of strike-slip and thrust for events within the plateau but at locations with surface elevations less than 5 km. For areas with surface elevations greater than 5 km, most events show normal faulting. Such a variation of source mechanism with elevation in Tibet was noted by MOLNAR and LYON-CAEN (1989) when they compiled fault plane solutions of 74 large earthquakes between 1962 and 1986. Our results, although only from one year of recording, demonstrate clearly the onset of normal faulting near the 5 km elevation (Fig. 9).

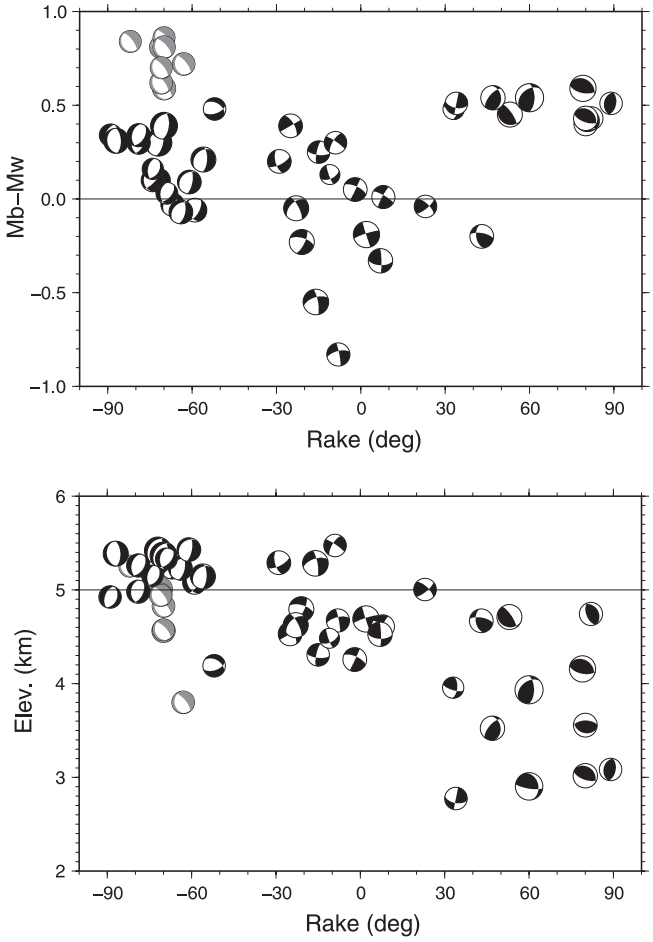

Figure 9
(A) Variation of $m_b - M_w$ with focal mechanism types. (B) Change of focal mechanisms with epicenter elevation. Focal spheres in gray shade are a cluster of earthquakes near station GANZ that exhibit anomalous m_b:M_w ratios.

6. Discussion and Conclusions

Our regional earthquake travel-time and waveform analyses show that the Tibetan plateau has a crustal thickness of 65 km with an average *P* velocity of 6.2–6.3 km/s. These values corroborate previous results from seismic data collected within the plateau (McNamara *et al.,* 1995; Rodgers and Schwartz, 1998; Zhao *et al.,*2001). The global average thickness and *P* velocity of the continental crust are 41.0 ± 6.2 km and 6.45 ± 0.21 km/s, respectively (Christensen and Mooney, 1995). Therefore, the Tibetan plateau has not only an anomalous thick crust but also

low crustal *P* velocity compared to the global average, which is unusual because under normal geotherm conditions, crustal material converts into high-density/high-velocity "mantle-like" mineral eclogites starting at a depth of about 50 km (e.g., ANDERSON, 1989). The low average crustal velocity of the Tibetan plateau suggests a steep geotherm, which is also supported by the high crustal Poisson's ratio (OWEN and ZANDT, 1997; ZHU, 1998), shallow seismicity cut-off depth (CHEN and MOLNAR, 1983; ZHAO and HELMBERGER, 1991; RANDALL *et al.,* 1995; LANGIN *et al.,* 2003), and widespread hot-springs and young volcanism throughout the plateau. Such a high geotherm gradient could be produced by the concentration of continental radiogenic crustal materials during crustal shortening (ZHAO and HELMBERGER, 1991) or by high heat flow from the upper mantle. LE PICHON *et al.,* (1997) used a simplified petrogenetic grid and a 1-D thermal model to calculate metamorphic transitions in the lower crust and their contribution to the uplift of Tibet. They found that a temperature of 1000°C is reached at the base of the crust after 30 to 80 Ma and all eclogites, if initially present, will be transformed to granulites in 18 to 45 Ma. The density reduction accompanied with the transformation will contribute ~3 km of post-thickening uplift.

There have been several seismic observations and interpretations that suggest a thin and warm mantle lithosphere beneath the central and northern Tibetan plateau (e.g., NI and BARAZANGI, 1983; MCNAMARA *et al.,* 1995; WITTLINGER *et al.,* 1996), which might be the locus of an upper mantle upwelling (MOLNAR, 1988). Our uppermost mantle *P* velocity of 8.1 km/s is consistent with previous results (CHEN and MOLNAR, 1981; MCNAMARA *et al.,* 1995; RODGERS and SCHWARTZ, 1998). Although it is close to the global average of 8.09 ± 0.20 km/s (CHRISTENSEN and MOONEY, 1995), it would be 7.93 km/s if the effect of overburden pressure due to the thick crust is corrected for (RODGERS and SCHWARTZ, 1998). Besides, the 8.1 km/s is an average over a large portion of the plateau. Seismic observations show that the upper mantle *P* and *S* velocities are slower in the central and northern plateau than in southern Tibet (e.g., NI and BARAZANGI, 1983; ZHAO and XIE, 1993; MCNAMARA *et al.,* 1995; RAPINE *et al.,* 2003). A relatively faster and colder mantle lithosphere beneath southern Tibet is also indicated by the existence of intermediate-depth (70 to 90 km) earthquakes under the Himalayas and near the Indo-Zangbu Suture (Fig. 8) (CHEN *et al.,* 1981; MOLNAR and CHEN, 1983; EKSTRÖM, 1987; CHEN, 1988; ZHU and HELMBERGER, 1996a). Whether these earthquakes occurred in the mantle lithosphere, given the abnormal crustal thickness of the plateau, has been questioned recently by MAGGI *et al.,* (2000); JACKSON (2002). The three earthquakes recorded by the one-year PASSCAL array were analyzed in detail by ZHU and HELMBERGER (1996a) using their broadband regional waveforms, and were concluded to be located 5 to 10 km below the Moho discontinuity. Given the short recording time period of the experiment, it is reasonable to suspect that more such subcrustal earthquakes exist. Effort should be taken to detect and map their spatial distribution.

Five km seems to be a critical elevation at which the Tibetan plateau can be maintained over long wavelengths. Normal-fault earthquakes occur where elevations are above this limit; an indication of crustal thinning and extension. The numerous large-scale NS-trending grabens in southern and central Tibet are most likely products of this extension over geological time (e.g., ARMIJO *et al.,* 1986). The beginning time of the EW extension and its relationship with the plateau uplift are not clear. One model suggests that the extension started when the thickened Tibetan mantle lithosphere was removed by a thermal instability, which subsequently lifted the surface elevation of the plateau from 3 km to 5 km (ENGLAND and HOUSEMAN, 1986; MOLNAR *et al.,* 1993). Others believe that the extension is much more recent and unrelated to large uplift increments (e.g., TAPPONNIER *et al.,* 2001). The coincidence of high topography with normal faulting merely implies large vertical stress that enhances rifting (ARMIJO *et al.,* 1986, 1989; TAPPONNIER *et al.,* 2001). TAYLOR *et al.,* (2003) proposed that rifts in the Qiangtang and Lhasa Terranes are kinematically linked by a series of conjugate sets of strike-slip faults along the Bangong Suture. We notice that most of our normal faulting earthquakes occurred in the Qiangtang terrane where the surface elevations are above 5 km and NS-trending grabens are less pronounced than those in the south (Fig. 8). As mentioned above, this is also where the current mantle lithosphere is believed to be thin and warm. Therefore, the normal faulting earthquakes may reflect the ongoing uplift and EW extension in the Qiangtang Terrane which might be related to a mantle lithosphere delamination underneath. These tectonic issues need to be addressed by future studies.

In summary, we have developed a simple but efficient multiple-event relocation method that does not employ a linearization approximation nor require an *a priori* velocity model. It uses first arrival times of events and iteratively estimates crust and upper mantle velocity parameters and relocates the events. We applied the method to 51 earthquakes in the Tibetan plateau recorded during a one-year PASSCAL seismic experiment. We found that on average, the crustal thickness of the plateau is about 65 km with a P velocity of 6.3 km/s. Average event relocation relative to the ISC locations, excluding two poorly located earthquakes, is 16 km. Their moment tensors and depths were also obtained by waveform inversion. All but one earthquake are at depths between 5 and 15 km. This is 15 km shallower, on average, than depths reported by ISC. The shallow seismicity cut-off depth and low crustal velocities suggest high temperatures in the lower crust. Thrust faulting source mechanisms dominate at the margins of the plateau. Within the plateau, but at locations with surface elevations less than 5 km, source mechanisms are a mixture of strike-slip and thrust. Almost all events occurring in the high plateau where elevations are above 5 km show normal faulting. This shows that a large portion of the plateau is under EW extension.

Acknowledgements

The authors are grateful to Brian Mitchell and Raul Madariaga whose comments have helped to improve the manuscript. LZ was partially supported by the NSF grant EA0439992.

REFERENCES

ANDERSON, D. L., *Theory of the Earth* (Blackwell Sci., Malden, Mass 1989).

ARMIJO, R., TAPPONNIER, P., MERCIER, J. L., and HAN, T. (1986), *Quaternary extension in southern Tibet: field observations and tectonic implications*, J. Geophys. Res. *91,* 13,803–13,872.

ARMIJO, R., TAPPONNIER, P., and HAN, T. (1989), *Late Cenozoic right-lateral strike-slip faulting in southern Tibet*, J. Geophys. Res. *94*, 2787–2838.

BARAZANGI, M., and NI, J. (1982), *Velocities and propagation characteristics of Pn and Sn beneath the Himalayan arc and Tibetan plateau: Possible evidence for underthrusting of Indian continental lithosphere beneath Tibet*, Geology *10*, 179–185.

BRANDON, C., and ROMANOWICZ, B. (1986), *A 'no-lid' zone in the central Chang-tang platform of Tibet: Evidence from pure path phase velocity measurement of long period Rayleigh waves*, J. Geophys. Res. *91*, 6547–6546.

CHEN, W. P. (1988), *A brief update on the focal depths of intracontinental earthquakes and their correlation with heat flow and tectonic age*, Seismol. Res. Lett. *59*, 263–272.

CHEN, W. P., and MOLNAR, P. (1981), *Constraints on the seismic wave velocity structure beneath the Tibetan Plateau and their tectonic implication*, J. Geophys. Res. *86*, 5937–5962.

CHEN, W. P., and MOLNAR, P. (1983), *Focal depths of intracontinental and intraplate earthquakes and their implications for the thermal and mechanical properties of the lithosphere*, J. Geophys. Res. *88*, 4183–4214.

CHEN, W. P., NABELEK, J. L., FITCH, T. J., and MOLNAR, P. (1981), *An intermediate depth earthquake beneath Tibet: Source characteristics of the event of September 14, 1976*, J. Geophys. Res. *86*, 2863–2876.

CHRISTENSEN, N. I., and MOONEY, W. D. (1995), *Seismic velocity structure and composition of the continental crust: A global view*, J. Geophys. Res. *100*, 9761–9788.

DEWEY, J. F., Shackleton, R. M., CHANG, C. and SUN, Y. (1988), *The tectonic evolution of the Tibetan Plateau*, Phil. Trans. R. Soc. Lond. *A327*, 379–413.

DOUGLAS, A. (1967), *Joint epicentre determination*, Nature, *215*, 45–48.

EKSTROM, G. (1987), *A broadband method of earthquake analysis*, Ph.D. thesis, Harvard Univ., Cambridge, Mass.

ENGLAND, P. C. and HOUSEMAN, G. A. (1986), *Finite strain calculations of continental deformation 2: Comparison with the India-Asia collision zone*, J. Geophys. Res. *91*, 3664–3676.

HARRISON, T. M., COPELAND, P., KIDD, W., and YIN, A. (1992), *Raising Tibet*, Science *255*, 1663–1670.

HELMBERGER, D. V. (1983), *Theory and application of synthetic seismograms*. In *Earthquakes: Observation, Theory and Interpretation*, pp. 174–222, Soc. Italiana di Fisica, Bolgna, Italy.

HIRN, A., NERCESSIAN, A., SAPIN, M., JOBERT, G., XU, Z. X., GAO, E. Y., LU, D. Y., and TENG, J. W. (1984a), *Lhasa block and bordering sutures - a continuation of a 500-km Moho traverse through Tibet*, Nature *307*, 25–27.

HIRN, A. *et al.* (1984b), *Crustal structure and variability of the Himalayan border of Tibet*, Nature *307*, 23–25.

INTERNATIONAL SEISMOLOGICAL CENTRE (2001), On-line bulletin, http://www.isc.ac.uk/Bull.

JACKSON, J. (2002), *Strength of the continental lithosphere: Time to abandon the jelly sandwich*?, GSA Today, September, 4–10.

JOBERT, N., JOURNET, B., JOBERT, G., HIRN, A., and Zhong, S. K. (1985), *Deep-structure of southern Tibet inferred from the dispersion of Raeyleigh-waves through a long-period seismic network*, Nature *313*, 386–388.

KANAMORI, H., MAECHLING, P., and HAUKSSON, E. (1999), Continuous monitoring of ground-motion parameters, *Bull. Seismol. Soc. Am. 89*, 311–316.

KISSLING, E., ELLSWORTH, W. L., EBERHART-PHILLIPS, D., and KRADOLFER, U. (1994), *Initial reference models in local earthquake tomography*, J. Geophys. Res. *99*, 19,635–19,646.

LANGIN, W. R., BROWN, L. D., and Sandvol, E. A. (2003), *Seismicity of central Tibet from project INDEPTH III seismic recordings*, Bull. Seismol. Soc. Am. *93*, 2146–2159.

LE PICHON, X., HENRY, P., and GOFFE, B. (1997), *Uplift of Tibet: from eclogites to granulites – implications for the Andean Plateau and the Variscan belt*, Tectonophys. *273*, 57–76.

LU, D., and WANG, X. (1990), *The crust structure and deep internal process in the Tuotuohe area of the north Qinghai-Xizang Plateau*, Bull. of the Chinese Academy of Geol. Sci. *21*, 227–237.

LYON-CAEN, H. (1986), *Comparison of the upper mantle shear-wave velocity structure of the Indian Shield and the Tibetan Plateau and tectonic implications*, Geophys. J. R. astr. Soc. *86*, 727–749.

MAGGI, A., JACKSON, J., PRIESTLEY, K., and BAKER, C. (2000), *A re-assessment of focal depth distributions in southern Iran, the Tien Shan and northern India: Do earthquakes really occur in the continental mantle*?, *Geophys. J. Int. 143*, 629–661.

MCNAMARA, D. E., OWENS, T. J., and WALTER, W. R. (1995), *Observations of regional phase propagation across the Tibetan plateau*, J. Geophys. Res. *100*, 22,215–22,229.

MOLNAR, P. (1988), *A review of geophysical constraints on the deep structure of the Tibetan plateau, the Himalaya and the Karakoram, and their tectonic implications*, Phil. Trans. R. Soc. Lond. *A326*, 33–88.

MOLNAR, P., and CHEN, W. P. (1983), *Focal depths and fault plane solutions of earthquakes under the Tibetan plateau*, J. Geophys. Res. *88*, 1180–1196.

MOLNAR, P., and LYON-CAEN, H. (1989), *Fault plane solutions of earthquakes and active tectonics of the Tibetan plateau and its margins*, Geophys. J. Int. *99*, 123–153.

MOLNAR, P., ENGLAND, P., and Martinod, J. (1993), *Mantle dynamics, uplift of the Tibetan plateau, and the Indian monsoon*, Rev. Geophys. *31*, 357–396.

NELSON, K. D. *et al.* (1996), *Partially molten middle crust beneath southern Tibet - synthesis of project INDEPTH results*, Science, *274*, 1684–1688.

NI, J., and BARAZANGI, M. (1983), *High-frequency seismic-wave propagation beneath the Indian shield, Himalayan arc, Tibetan plateau and surrounding regions – high uppermost mantle velocities and efficient Sn propagation beneath Tibet*, Geophys. J. R. astr. Soc. *72*, 665–689.

OWENS, T. J., and ZANDT, G. (1997), *Implications of crustal property variations for models of Tibetan plateau evolution*, Nature *387*, 37–43.

OWENS, T. J., RANDALL, G. E., WU, F. T., and R. S. ZENG (1993), *PASCAL instrument performance during the Tibetan plateau passive seismic experiment*, Bull. Seismol. Soc. Am. *83*, 1959–1970.

PAVLIS, G. L., and BOOKER, J. R. (1983), *Progressive multiple event location (PMEL)*, Bull. Seismol. Soc. Am. *73*, 1753–1777.

RANDALL, G. E., AMMON, C. J., and OWENS, T. J. (1995), *Moment-tensor estimation using regional seismograms from portable network deployments*, Geophys. Res. Lett. *22*, 1665–1668.

RAPINE, R., TILMANN, F., WEST, M., and NI, J. (2003), *Crustal structure of northern and southern Tibet from surface wave dispersion analysis*, J. Geophys. Res. *108*, 2120, doi:10.1029/2001JB000445.

RICHARDS-DINGER, K. B., and SHEARER, P. M. (2000), *Earthquake locations in southern california obtained using source-specific station terms*, J. Geophys. Res. *105*, 0939–10,960.

RODGERS, A., and SCHWARTZ, S. Y. (1997), *Low crustal velocities and mantle lithospheric variation in southern Tibet from regional Pnl waveforms*, Geophys. Res. Lett. *25*, 9–12.

RODGERS, A., J., and SCHWARTZ, S. Y. (1998), *Lithospheric structure of the Qiangtang Terrane, northern Tibetan Plateau, from complete regional waveform modeling: Evidence for partial melt*, J. Geophys. Res. *103*, 7137–7152.

ROMANOWICZ, B. (1982), *Constraints on the structure of the Tibet plateau from pure path phase velocities of Love and Rayleigh-waves*, J. Geophys. Res. *87*, 6865–6883.

ROSS, A. R., BROWN, L. D., PANANONT, P., NELSON, K. D., KLEMPERER, S., HAINES, S., ZHAO, W., and GUO, J. (2004), *Deep reflection surveying in central Tibet: lower-crustal layering and crustal flow*, Geophys. J. Int. *156*, 115–128.

SONG, X. J., HELMBERGER, D. V., and ZHAO, L. (1996), *Broadband modeling of regional seismograms: The Basin and Range crustal structure*, Geophys. J. Int. *125*, 15–29.

TAN, Y., ZHU, L., HELMBERGER, D. V., and SAIKIA, C. K. (2006), *Locating and modeling regional earthquakes with two stations*, J. Geophys. Res. *111*, B01306, doi: 10.1029/2005JB003775.

TAPPONNIER, P., XU, Z., ROGER, F. MEYER, B., ARNAUD, N., WITTLINGER, G., and YANG, J. (2001), *Oblique stepwise rise and growth of the Tibet Plateau, Science*, *294*, 1671–1677.

TAYLOR, M., YIN, A., RYERSON, F. J., KAPP, P., and LIN, D. (2003), *Conjugate strike-slip faulting along the Bangong-Nujiang suture zone accommodates coeval east-west extension and north-south shortening in the interior of the Tibetan Plateau*, Tectonics, *22*, 1044, doi:10.1029/2002TC001361.

TENG, J., XIONG, S., YIN, Z., XU, Z., WANG, X., and LU, D. (1983), *Structure of the crust and upper mantle pattern and velocity distribution characteristic at northern region of the Himalayan mountains*, Acta. Geophys. Sinica. *26*, 525–540.

VERGNE, J., WITTLINGER, G., HUI, Q., TAPPONNIER, P., POUPINET, G., MEI, G. J., HERQUEL, G., and Paul, A. (2002), *Seismic evidence for stepwise thickening of the crust across the NE Tibetan Plateau*, Earth Planet. Sci. Lett. *203*, 25–33.

WITTLINGER, G., *et al.* (1996), *Seismic tomography of northern Tibet and Kunlun: Evidence for crustal blocks and mantle velocity contrasts*, Earth Planet. Sci. Lett. *139*, 263–279.

YIN, A., and NIE, S. *A Phanerozoic palinspastic reconstruction of China and its neighboring regions*. In *Tectonic evolution of Asia* (eds. A. Yin and T. M. Harrison), pp. 442–485, (Cambridge Univ. Press 1996).

YUAN, X., NI, J., KIND, R., MECHIE, J., and SANDVOL, E. (1997), *Lithospheric and upper mantle structure of southern Tibet from a seismological passive source experiment*, J. Geophys. Res. *102*, 27,491–27,500.

ZHAO, L. S., and HELMBERGER, D. V. (1991), *Geophysical implication from relocation of Tibetan earthquakes; hot lithosphere*, Geophys. Res. Lett. *18*, 1070–1084.

ZHAO, L. S., and HELMBERGER, D. V. (1994), *Source estimation from broadband regional seismograms*, Bull. Seismol. Soc. Am. *84*, 91–104.

ZHAO, L. S., and XIE, J. (1993), *Lateral variation in compressional velocities beneath the Tibetan plateau from Pn travel-time tomography*, Geophys. J. Int. *115*, 1070–1084.

ZHAO, L. S., HELMBERGER, D. V., and HARKRIDER, D. G. (1991), *Shear-velocity structure of the crust and upper mantle beneath the Tibetan plateau and southeastern China*, Geophys. J. Int. *105*, 713–730.

ZHAO, W., NELSON, K. D., and TEAM, P. I. (1993), *Deep seismic reflection evidence for continental underthrusting beneath southern Tibet*, Nature *366*, 557–559.

ZHAO, W. *et al.* (2001), *Crustal structure of central Tibet as derived from project INDEPTH wide angle seismic data*, Geophys. J. Int. *145*, 486–498.

ZHU, L. (1998), *Broadband waveform modeling and its application to the lithospheric structure of the Tibetan Plateau*, Ph.D. thesis, California Institute of Technology, Pasadena.

ZHU, L., and HELMBERGER, D. V. (1996a), *Intermediate depth earthquakes beneath the India-Tibet collision zone*, Geophys. Res. Lett. *23*, 435–438.

ZHU, L., and HELMBERGER, D. V. (1996b), *Advancement in source estimation techniques using broadband regional seismograms*, Bull. Seismol. Soc. Am. *86*, 1634–1641.

ZHU, L., and RIVERA, L. A. (2002), *A note on the dynamic and static displacements from a point source in multi-layered media*, Geophys. J. Int. *148*, 619–627.

(Received June 1, 2005, accepted November 8, 2005)
Published Online First: June 27, 2006